MNRAS 000, 1–11 (2019) Preprint 28 November 2019 Compiled using MNRAS LATEX style file v3.0

Asteroseismic masses of four evolved planet-hosting stars using SONG and TESS: resolving the retired A-star mass controversy

Sai Prathyusha Malla[1]★ Dennis Stello[1,2,3] Daniel Huber[4] Ben Montet[1] Timothy R. Bedding[2,3] Mads Fredslund Andersen[3], Frank Grundahl[3] Daniel R. Hey[2,3] Pere L. Palle[5,6] Licai Deng[7] Chunguang Zhang[7] Xiaodian Chen[7] James Lloyd[8] Victoria Antoci[3]

[1]*School of Physics, The University of New South Wales, Sydney NSW 2052, Australia*
[2]*Sydney Institute of Astronomy(SIfA), School of Physics, University of Sydney, NSW 2006, Australia*
[3]*Stellar Astrophysics Centre, Dept. of Physics and Astronomy, Aarhus University, Ny Munkegade, DK- 8000 Aarhus C, Denmark.*
[4]*Institute for Astronomy, University of Hawai'i, 2680 Woodlawn Drive, Honolulu, HI 96822, USA*
[5]*Instituto de Astrofísica de Canarias, E-38200 La Laguna, Tenerife, Spain*
[6]*Universidad de La Laguna (ULL), Departamento de Astrofísica, E-38206 La Laguna, Tenerife, Spain*
[7]*Key Laboratory of Optical Astronomy, National Astronomical Observatories, Chinese Academy of Sciences, Beijing 100101, People's Republic of China*
[8]*Department of Astronomy, Cornell University, Ithaca, NY 14850, USA*

Accepted XXX. Received YYY; in original form ZZZ

ABSTRACT

The study of planet occurrence as a function of stellar mass is important for a better understanding of planet formation. Estimating stellar mass, especially in the red giant regime, is difficult. In particular, stellar masses of a sample of evolved planet-hosting stars based on spectroscopy and grid-based modelling have been put to question over the past decade with claims they were overestimated. Although efforts have been made in the past to reconcile this dispute using asteroseismology, results were inconclusive. In an attempt to resolve this controversy, we study four more evolved planet-hosting stars in this paper using asteroseismology, and we revisit previous results to make an informed study of the whole ensemble in a self-consistent way. For the four new stars, we measure their masses by locating their characteristic oscillation frequency, $\nu_{\rm max}$, from their radial velocity time-series observed by SONG. For two stars, we are also able to measure the large frequency separation, $\Delta\nu$, helped by new observations from TESS and extended SONG single-site and dual-site observations. We establish the robustness of the $\nu_{\rm max}$-only-based results by independently determining the stellar mass from $\Delta\nu$, and from both $\Delta\nu$ and $\nu_{\rm max}$. We then compare the seismic masses of the full ensemble of 16 stars with the spectroscopic masses from three different literature sources. We find an offset between the seismic and spectroscopic mass scales that is mass-dependent, suggesting that the previously claimed overestimation of spectroscopic masses only affects stars more massive than about 1.6 $M_\odot$.

Key words: keyword1 – keyword2 – keyword3

1 INTRODUCTION

The study of planet occurrence as a function of host star properties, in particular stellar mass, can improve our understanding of planet formation. For this, we need to study potential planet hosts in a range of stellar masses. However, finding planets around main-sequence stars that are more massive than about 1.4 $M_\odot$ can be challenging, particularly for the radial velocity technique because of the increased line broadening induced by the faster rotation of these stars. To overcome this, Johnson et al. (2006) set out to target intermediate-mass stars in the subgiant and red giant evolution phase, which are more favourable to planet detection using radial velocity measurements. These stars, which they dubbed 'retired A-stars', were inferred to be the descendants of main-sequence A- or hot F-type stars.

To find which giants are the descendants of main-sequence A- and hot F-type stars require estimates of stellar mass. However, stellar mass is notoriously difficult to obtain for red giants and late subgiants. It is typically estimated by interpolating observed stellar properties such as absolute magnitude and, typically spectroscopy-

★ E-mail: s.malla@student.unsw.edu.au (UNSW)

based metallicity ([Fe/H]), effective temperature ($T_{\rm eff}$), and surface gravity ($\log g$) onto stellar model grids (Prieto & Lambert 1999; Pont & Eyer 2004). However, the stellar models of a large range of masses converge in the red giant regime of the HR-diagram such that models with different evolution speeds are within the observed error box. This led Lloyd (2011) to question the inferred masses of the so-called retired A-star sample, predicting they could be overestimated by up to 50% (based on a selection of evolved planet-hosting stars from the Exoplanet Orbit Database[1], Wright et al. 2011).

Later, Johnson et al. (2013) applied an apparent magnitude limit on their sample of subgiants and benchmarked them against a Galactic stellar population model to show that there was no overestimation in the spectroscopic masses of these evolved planet-hosting stars. The imposed apparent magnitude limit increased the relative number of massive stars ($M \gtrsim 1.5\,{\rm M}_{\odot}$) observed in their target sample, and hence Johnson et al. (2013) argued that this limit partially counteracts the otherwise lower number of massive stars expected from their faster evolution. However, Lloyd (2013) repeated the calculation in Lloyd (2011), now using apparent magnitude-limited weights for the isochrone integration. From these recalculations, Lloyd (2013) showed that there are fewer massive stars than found in literature, irrespective of the limit used in the target selection (volume- or magnitude-limit). Meanwhile, Schlaufman & Winn (2013) determined model-independent masses from space velocity dispersions. They found that the velocity dispersions of their subgiant sample were larger than for their main-sequence A0-F5 stars but consistent with their main sequence F5-G5 sample. Hence, they concluded that their evolved planet-hosting stars are less massive than A0-F5 stars, in agreement with Lloyd (2011). Due to the conflicting results obtained, the debate continued about what the true masses of these evolved planet-hosting stars were.

While classical spectroscopically-based mass determinations can be challenging due to the relatively large uncertainties on the spectroscopic parameters like effective temperature, metallicity and surface gravity ($\log g$), recent breakthroughs in asteroseismology have demonstrated that using asteroseismic measurements can provide more precise stellar masses (Huber et al. 2012; Gaulme et al. 2016; Huber et al. 2017; Yu et al. 2018), independent of stellar models (Stello et al. 2008; Kallinger et al. 2010; Chaplin & Miglio 2013; Basu & Chaplin 2018). Thus, asteroseismology is an obvious approach to resolve the dispute over the masses of these evolved planet-hosting stars.

Despite the precision of asteroseismology, the masses of these stars are still contentious. Johnson et al. (2014) made the first attempt to study the only star (HD 185351) in the *Kepler* field that was among the known intermediate-mass evolved planet-hosting stars previously found by radial-velocity (hence amenable to asteroseismic investigation). Unfortunately, only one month of *Kepler* data was available, and no definite conclusion could be made because no unique solution could reconcile all (spectroscopic, seismic, and interferometric) measurements at hand. However, a follow-up study (Hjørringgaard et al. 2017) with a more comprehensive analysis of the asteroseismic data and associated modelling found a unique solution that reconciled all measurements. They concluded that the disputed spectroscopy-based mass was overestimated by about 15%. Stello et al. (2017) also found that the spectroscopic masses of seven of the eight evolved planet-hosting stars they studied with the ground-based Stellar Observations Network Group (SONG) telescope (Andersen et al. 2016) were 15-20% higher than their corresponding seismic masses. White et al. (2018) determined the masses of 5 evolved planet-hosts based on interferometry and also found the spectroscopic masses from the literature to be 15% larger than their values. Campante et al. (2017) and North et al. (2017) found no apparent difference between the spectroscopic and seismic masses in their sample of stars (not all planet-hosting) observed by K2. Similarly, Ghezzi et al. (2018) found the difference between the spectroscopic and seismic mass scales insignificant compared to the uncertainty in the stellar masses they obtained.

In this paper, we further investigate the masses of the evolved planet-hosting stars that were previously called into question. For this purpose, we observed four evolved planet-hosting stars for 1-2 weeks each using the Tenerife node of the SONG telescope. We used the oscillations to estimate the stellar masses following the approach by Stello et al. (2017). In addition to this nominal observing strategy, we observed one star, γ Cep, for two months from the SONG telescope at Tenerife and we observed the same star again simultaneously from two SONG nodes (Tenerife and Delingha, China) for about three weeks. We use the data from these two independent observations to check the robustness of the initial 1-2 week-based SONG data. We then verify our findings of the SONG-based seismic masses against the seismic mass obtained from the *Transiting Exoplanet Survey Satellite* (TESS) (Ricker et al. 2016) for one of the stars in our sample, 24 Sex. Finally, we combine the results from our seismic analysis with those of Stello et al. (2017) and North et al. (2017) to form an ensemble of 16 stars; this allows us to make the most comprehensive seismic-based analysis of the retired A-star mass controversy to date.

2 TARGET SELECTION AND OBSERVATIONS

We selected our targets from the Exoplanet Orbit Database, which had been the basis for the mass controversy. We used the same selection criteria as Stello et al. (2017) in effective temperature and luminosity (L): $3.65 < \log(T_{\rm eff}/{\rm K}) < 3.75$ (i.e. 4467 K $> T_{\rm eff} >$ 5623 K) and $\log(L/{\rm L}_{\odot}) > 0.75$ ($L > 5.62\,{\rm L}_{\odot}$). The luminosity of the target was derived from a metallicity-dependent bolometric correction equation (Alonso et al. 1999, Eq. 18) assuming negligible extinction, given the proximity of the targets (see Stello et al. (2017) for details). From this initial selection, we chose the four brightest stars with $\log g > 3$ that were not already targeted by Stello et al. (2017). Fig. 1 shows our four new targets, along with solar metallicity stellar evolution tracks from Stello et al. (2013) derived using MESA (Paxton et al. 2013) with dots spaced equally in age.

We used the SONG nodes in Tenerife (Andersen et al. 2014; Grundahl et al. 2017) and Delingha (Deng et al. 2012) for the observations. Observations made at Tenerife used the échelle spectrograph of the robotic 1-metre Hertzsprung SONG telescope operated in a fully automated mode (Fredslund Andersen et al. 2019). Observations made at Delingha used a similar spectrograph, but with a slightly shorter spectral range. The operation of the Delingha telescope was not automated, and the observations were carried with an observer present. An iodine cell was used at both nodes for precise wavelength calibration.

The four new stars in our sample were observed for about 10 days from March to August 2018. In addition to the four new stars, we also observed γ Cep (which was observed by Stello et al. (2017) for 13 days) for a period of 75 days from August to November 2014, and using the SONG telescopes from Tenerife and Delingha simultaneously for 24 days from October to November 2017. We

[1] www.exoplanets.org

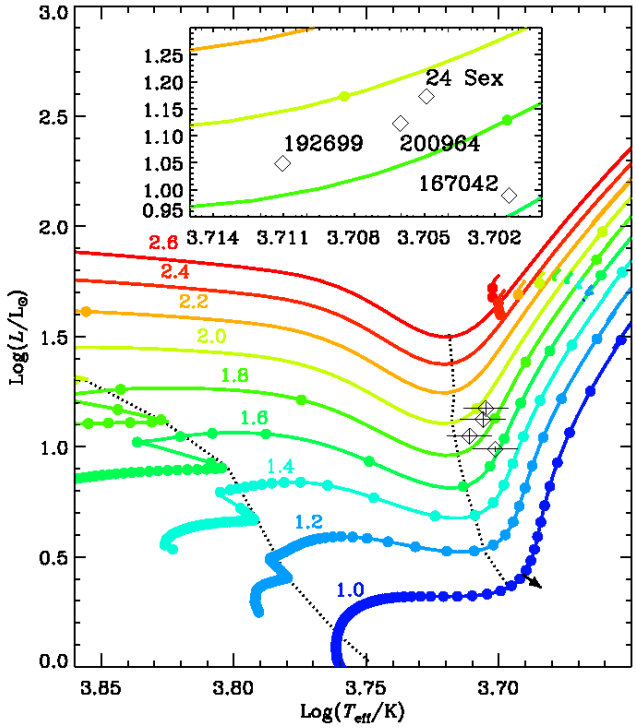

Figure 1. The HR-diagram shows the stellar evolution tracks from MESA (Paxton et al. 2013) of solar metallicity from Stello et al. (2013). The filled dots along each track indicate the likelihood of finding a star in a given state of evolution, each separated by 50 million years in stellar age. All masses represented in the figure are is solar units. The track shift when the [Fe/H] is increased by 0.2 dex is shown by the black arrow near the bottom of the 1.0 $M_\odot$ red giant branch. The dotted fiducial lines indicate the transitions from the main-sequence to subgiants, and from the rapidly cooling subgiants at roughly the same radius to the rapidly expanding red giants at approximately the same $T_{\rm eff}$. The planet-hosting targets are represented by diamonds, and the black lines indicate the corresponding uncertainties in their luminosities and effective temperatures. The models within the range of luminosities 1.6 $\lesssim \log(L/L_\odot) \lesssim$ 1.8 are the helium-core burning ones. The inset shows a close-up of where the targets lie on the HR-diagram.

Table 1. Observing parameters for targets (all Tenerife except where noted)

Star ID	Observation dates	m_v	T_{exp} [s]	N_{exp}	R	N^{obs}_{night} [days]	N^{span}_{night} [days]	σ_{RV} [m/s]
24 Sex	05/03 - 17/03/18	6.44	600	404	77k	10	12	6.70
HD 167042	01/06 - 11/06/18	5.95	900	311	90k	10	10	1.77
HD 192699	27/07 - 11/08/18	6.45	1200	128	90k	8	16	3.37
HD 200964	17/08 - 27/08/18	6.49	1200	205	90k	11	11	2.96
γ Cep (2014)	30/08 - 14/11/14	3.21	180	1264	90k	62	75	2.00
γ Cep	30/10 - 24/11/17	3.21	180	860	90k	20	23	2.60
γ Cep (Delingha)	30/10 - 22/11/17	3.21	180	2427	90k	21	24	4.54

m_v : magnitude
T_{exp} : exposure time
N_{exp} : number of exposures
R : spectrograph resolution
N^{obs}_{night}: number of observation nights
N^{span}_{night}: length of time-series
σ_{RV} : median radial velocity precision

combined the dual-site data by shifting each series to a common radial velocity zero-point. The observing parameters are listed in Table 1.

The extraction of 1-D spectra and the calculation of radial velocities used the same method as Grundahl et al. (2017). The 1-D spectra were extracted using a pipeline based on the IDL routines by Piskunov & Valenti (2002) and Ritter et al. (2014). The radial velocities were then calculated following the approach by Butler et al. (1996) implemented in the *iSONG* software (Antoci et al. 2013; Grundahl et al. 2017). The radial velocity time-series were passed through a high-pass filter with a cutoff frequency of ~ 3 μHz to prevent power leakage in the frequency range of stellar oscillations due to the presence of any slow-moving trends in the data. The final time-series after performing a 3σ-clipping are shown in Figs. 2 and 3.

The radial velocity variations are typically about ± 10 m/s and dominated by the oscillations as seen in the inset showing a single-night close-up for HD 192699 (Fig. 2c). The radial velocity time-series for the single-site (2014) data and the dual-site data for γ Cep are shown in Fig. 3.

We also obtained high-precision photometric data from TESS for one of our four new stars, 24 Sex. This star was observed in 2-min cadence in Sector 8 from 2 to 27 February 2019. We downloaded the data from MAST[2] and used the corrected light curve (PDCMAP) for our analysis. The photometric time-series was treated in a similar way to the radial velocity time-series, the only exception being the application of a high-pass filter with a cutoff frequency of ~ 50 μHz due to the larger noise levels at lower frequencies for photometric observations. The high-pass filtered time-series of the TESS data for 24 Sex is illustrated in Fig. 4a.

3 MEASURING ν_{max} AND ITS UNCERTAINTY

Similar to Stello et al. (2017), we used the same method as Huber et al. (2009) to locate the frequency of maximum acoustic power, ν_{max}. In detail, we obtained the power spectra of the radial velocity time-series using a discrete weighted Fourier transform. The resulting power spectra are shown in Figs. 4b, 5 and 6.

Using a large frequency separation, $\Delta\nu$, estimated from the $\Delta\nu - \nu_{max}$ relation (Stello et al. 2009, Eq. 1), we smoothed the power spectrum with a $4\Delta\nu$ wide Gaussian. The highest point of the heavily smoothed power spectrum was taken as ν_{max} (Fig. 5, red dot), and the values are tabulated in Table 2 (column 9). We tested that the exact choice of the Gaussian smoothing width did not significantly affect our final ν_{max} determination. The test was conducted by varying the Gaussian width by ± 50% (corresponding to $2\Delta\nu$), which changed the final ν_{max} estimate by no more than ± 2% for three out of the five stars in our sample. For one star HD 167042, the change was ± 5% due to its broader excess power in the oscillation spectrum. We also note that correcting for any power-loss due to the averaging effect on oscillations during the integration time, like in the case of *Kepler* long-cadence data (Murphy 2012, Eq. 1), only changes the ν_{max} by $\lesssim$ 1%. Further, Stello et al. (2017) note that their inferred ν_{max} values did not change significantly (less than 1%) whether or not one takes the stellar background noise into account (see Stello et al. (2017) for details). This is because the background is very low in radial velocity measurements.

[2] https://mast.stsci.edu/portal/Mashup/Clients/Mast/Portal.html

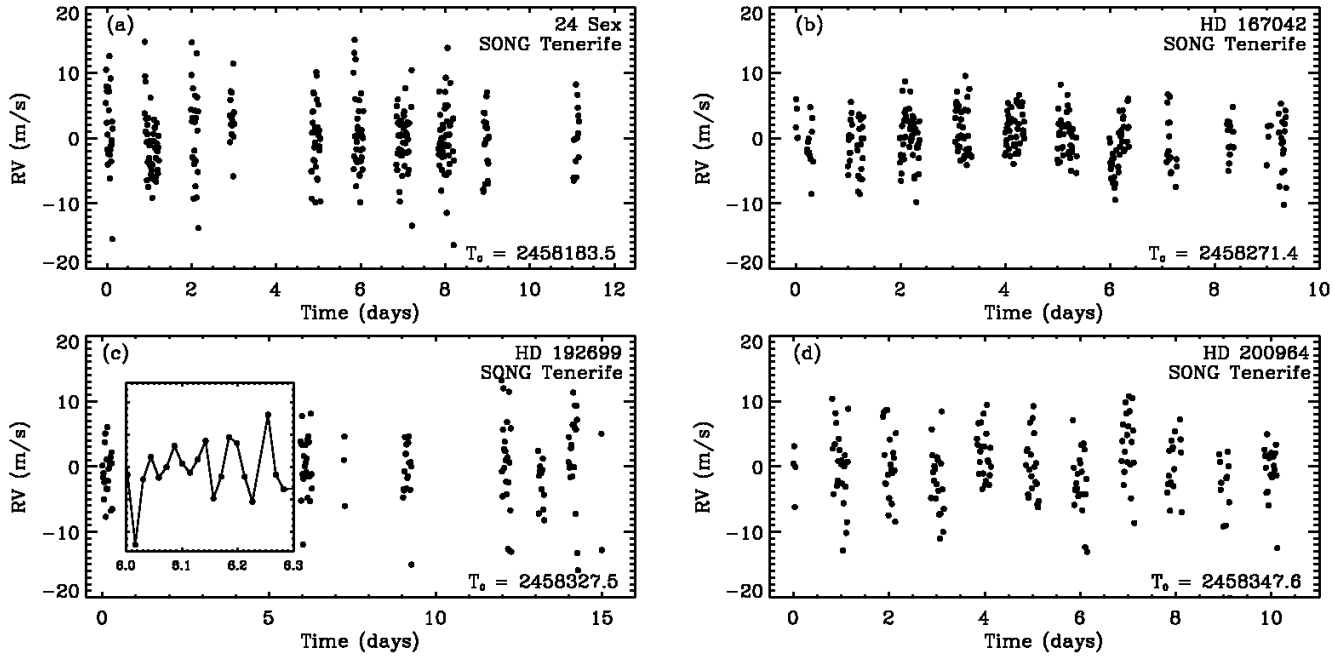

Figure 2. Radial velocity time-series for the four new evolved planet-hosting stars studied in this paper. For HD 192699, a single night of observations is shown in the inset. T_0 is the time (BJD) of the first data point. The data can be acquired from the SONG Data Archive (SODA) or from the author upon request.

Table 2. Observed parameters of the evolved planet-hosting stars

	Literature					Derived		Asteroseismology	
Star name	$\log g$ [dex]	$T_{\rm eff}$ [K]	[Fe/H] [dex]	π [mas]	M [$M_\odot$]	L [$L_\odot$]	$\nu_{\rm max,pre}$ [μHz]	$\nu_{\rm max,obs}$ [μHz]	M [$M_\odot$]
(1)	(2)[a]	(3)[a]	(4)[a]	(5)[b]	(6)[a]	(7)	(8)	(9)	(10)[c]
24 Sex	3.40 ± 0.13	5069 ± 62	-0.01 ± 0.05	12.91 ± 0.38	1.81 ± 0.08	14.90 ± 0.92	238 ± 24	203 ± 10	1.55 ± 0.16
HD 167042	3.35 ±0.18	5028 ± 53	0.03 ± 0.04	19.91 ± 0.26	1.63 ± 0.06	9.75 ± 0.27	318 ± 26	281 ± 14	1.44 ± 0.13
HD 192699	3.45 ± 0.07	5141 ± 20	-0.2 ± 0.02	15.24 ± 0.57	1.58 ± 0.04	11.18 ± 0.92	290 ± 30	208 ± 10	1.13 ± 0.13
HD 200964	3.41 ± 0.08	5082 ± 38	-0.2 ± 0.03	13.85 ± 0.52	1.57 ± 0.06	13.28 ± 1.09	233 ± 27	170 ± 8	1.14 ± 0.14

[a] Source: Exoplanet Orbit Database, which refers to Mortier et al. (2013). Similar to Stello et al. (2017), we assume $\sigma_{T_{\rm eff}}$ = 100 K and $\sigma_{\rm [Fe/H]}$ = 0.1 dex to derive columns 7-8 and 10 instead of the quoted uncertainties in $T_{\rm eff}$ and [Fe/H] (Thygesen et al. 2012).
[b] Source: *Hipparcos* (Leeuwen 2007)
[c] $\nu_{\rm max}$-only based asteroseismic masses

3.1 Estimating $\nu_{\rm max}$ uncertainty

Stello et al. (2017) adopted a 15% assumed $\nu_{\rm max}$ uncertainty based on their investigation of the old ξ Hya data obtained using the Coralie spectrograph on the Euler Telescope (which has a similar performance as SONG) at La Silla (Frandsen et al. 2002). However, here we do not just adopt this 15% $\nu_{\rm max}$ uncertainty.

We now have longer SONG time-series for two of the planet-hosting stars reported by Stello et al. (2017): (1) the 75-day long γ Cep data presented in Fig. 3a (2) as well as the 110-day long ϵ Tau data from Arentoft et al. (2019). This allows us to divide these long series into shorter segments, each similar in length to those of our main sample of stars (about 10 days). By measuring the scatter in $\nu_{\rm max}$ across segments, we can get a realistic estimate of the uncertainty in $\nu_{\rm max}$. This approach is essentially the same as by Stello et al. (2017) (with their ξ Hya data). However, in our case, the instrumentation and the data reduction approach are identical to that of our shorter observation data sets.

We split the 75-day long single-site γ Cep time-series into segments of 10 days and measure their $\nu_{\rm max}$ treating them as described in Sec. 3. We observe a $\nu_{\rm max}$ scatter of 2.5% across these segments. For the 110-day ϵ Tau data, we found a $\nu_{\rm max}$ scatter of 5% also using 10-day segments. Based on the above test on γ Cep and ϵ Tau, we adopt a 5% $\nu_{\rm max}$ uncertainty for our four new targets, which is also a typical uncertainty for $\nu_{\rm max}$ from photometry (e.g., Huber et al. 2011).

We note that our adopted 5% $\nu_{\rm max}$ uncertainty is three times smaller than the 15% $\nu_{\rm max}$ uncertainty used by Stello et al. (2017) from their analysis of the ξ Hya radial velocity time-series. ξ Hya is in a different phase of evolution (secondary clump star) and oscillates at much lower frequencies compared to γ Cep or ϵ Tau. As a result, it has a relatively wide envelope of oscillation power (Yu et al. 2018) and the data is not densely sampled, leading to a much lower signal-to-noise ratio. These factors may contribute to the larger intrinsic $\nu_{\rm max}$ scatter. In Sec. 6, we adopt the mass

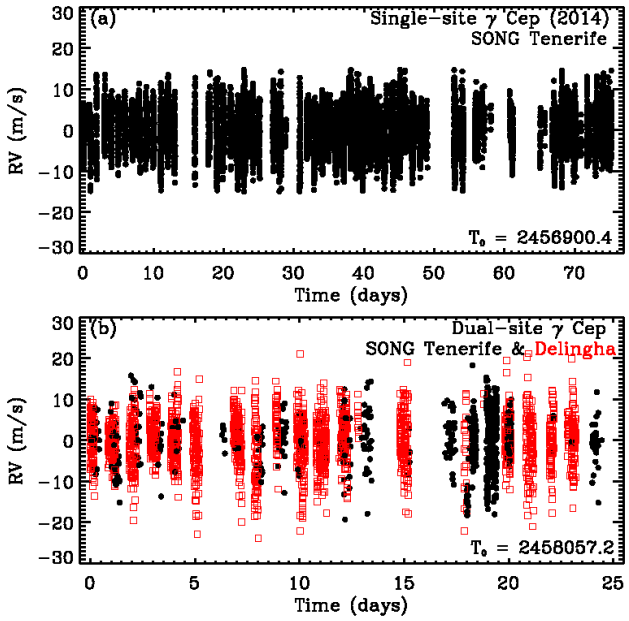

Figure 3. (a) Radial velocity time-series for single-site γ Cep, which was observed for a period of 75 days from the SONG node at Tenerife. T_0 is the time (BJD) of the first data point. (b) Combined radial velocity time-series for the dual-site γ Cep observations. The filled black circles represent the data from Tenerife while unfilled red squares represent the data from Delingha. The data can be acquired from the SONG Data Archive (SODA) or from the author upon request.

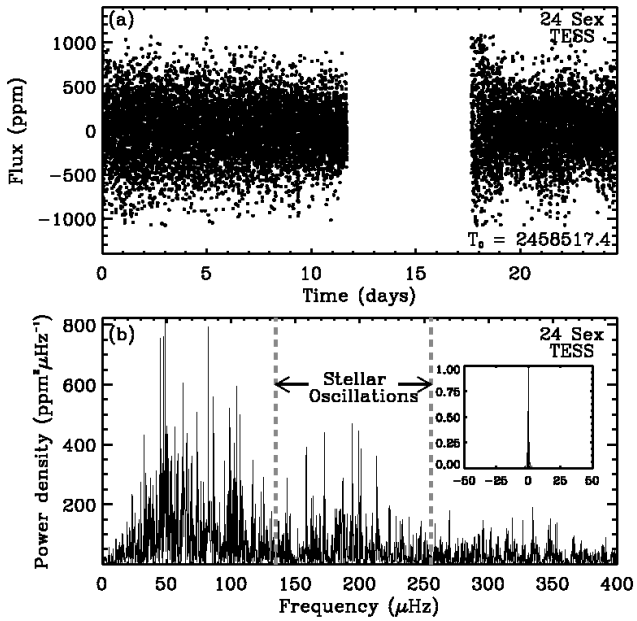

Figure 4. (a) TESS Light curve of 24 Sex. A high-pass filter of 50 μHz is applied. T_0 is the time (BJD) of the first data point. The data used here can be obtained from `http://dx.doi.org/10.17909/t9-fnwn-cr91`. (b) Corresponding power density spectrum. The spectral window is in the inset.

Table 3. Updated Results from Stello et al. (2017)

Star name	$\nu_{\rm max}$ (μHz)	M ($M_\odot$)
(1)	(2)	(3)
ϵ Tau	56.9 ± 2.9	2.40 ± 0.22
β Gem	84.5 ± 4.2	1.73 ± 0.17
18 Del	112 ± 6	1.92 ± 0.19
γ Cep	185 ± 9	1.32 ± 0.12
HD 5608	181 ± 9	1.32 ± 0.13
κ CrB	213 ± 11	1.40 ± 0.12
6 Lyn	183 ± 9	1.37 ± 0.14
HD 210702	223 ± 11	1.47 ± 0.14

estimates by Stello et al. (2017) for our ensemble analysis, using our newly derived 5% uncertainties. We, therefore, provide an updated summary of the results from Stello et al. (2017) with this fractional uncertainty in Table 3.

4 DERIVING STELLAR MASSES

To calculate stellar seismic mass from the observed $\nu_{\rm max}$, we used the following scaling relation (Brown et al. 1991; Kjeldsen & Bedding 1995):

$$\frac{\nu_{\rm max}}{\nu_{\rm max,\odot}} \simeq \frac{M}{M_\odot}\left(\frac{T_{\rm eff}}{T_{\rm eff,\odot}}\right)^{3.5}\left(\frac{L}{L_\odot}\right)^{-1}. \quad (1)$$

Here we used $\nu_{\rm max,\odot}$ = 3090 μHz and $T_{\rm eff,\odot}$ = 5777K (Huber et al. 2009) to be consistent with Stello et al. (2017). We used *isoclassify*[3] (Huber et al. 2017) to compute the luminosity of the stars in our sample using the spectroscopic $T_{\rm eff}$ from the Exoplanet Orbit Database (Table 2, Column 3), *Hipparcos*[4] parallax (Table 2, Column 5) and Tycho V_T photometry as inputs. We set the *dustmap* parameter to 'allsky', which enables the use of a combination of reddening maps from Drimmel et al. (2003), Marshall et al. (2006), Green et al. (2015) and Bovy et al. (2016) implemented in the *mwdust* package by Bovy et al. (2016). The luminosity and the seismic mass are tabulated in Table 2 (columns 7 and 10).

We note that the location of the seismic signal predicted from the same scaling relation (Eq. 1) using the spectroscopic $T_{\rm eff}$ and masses from the Exoplanet Orbit Database is consistently larger than the observed $\nu_{\rm max}$ (Fig. 5, dashed blue line). The predicted $\nu_{\rm max}$ is tabulated in Table 2 (column 8). Likewise, the seismic masses based on $\nu_{\rm max}$ (through Eq. 1) are lower than their spectroscopic counterparts for all the four new stars in our sample.

5 LARGE FREQUENCY SEPARATION OF γ Cep AND 24 SEX

Support for our $\nu_{\rm max}$-based masses could come from measurements of masses from the frequency separation between overtone modes, $\Delta\nu$, which scales with the square root of the mean stellar density. Hence,

$$\frac{\Delta\nu}{\Delta\nu_\odot} \simeq \left(\frac{M}{M_\odot}\right)^{0.5}\left(\frac{L}{L_\odot}\right)^{-0.75}\left(\frac{T_{\rm eff}}{T_{\rm eff,\odot}}\right)^{3}. \quad (2)$$

[3] `https://github.com/danxhuber/isoclassify`

[4] We use *Hipparcos* because for brighter stars (G < 5), Gaia DR2 is known to have significant systematic errors due to calibration issues (Drimmel et al. 2019)

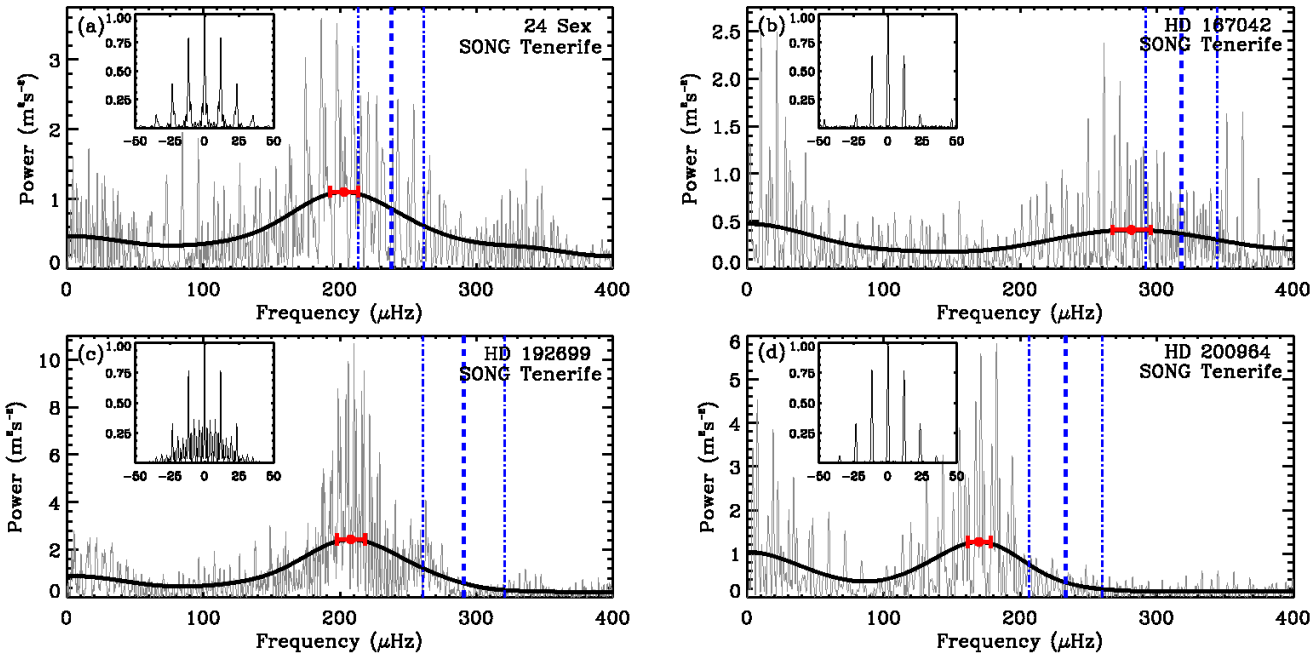

Figure 5. Power spectra of the four new planet-hosting stars observed by SONG. The thick black line is the power spectrum smoothed using a Gaussian of width 4-$\Delta\nu$. The red dot and the 1σ error bars show the observed $\nu_{\rm max}$. The thick dashed blue line represents the $\nu_{\rm max}$ predicted from Eq. 1 using the spectroscopic $T_{\rm eff}$ and mass from the Exoplanet Orbit Database (Table 2, column 8) and the thinner dot-dash blue lines represent the corresponding uncertainty. The spectral windows are plotted in the insets.

This provides independent measurements of stellar masses from $\nu_{\rm max}$ and $\Delta\nu$ to check if our results are consistent. We can also combine $\Delta\nu$ (Eq. 2) with $\nu_{\rm max}$ (Eq. 1) to give a mass with very little $T_{\rm eff}$ dependence,

$$\frac{M}{\rm M_\odot} \simeq \left(\frac{\nu_{\rm max}}{\nu_{\rm max,\odot}}\right)^{3} \left(\frac{\Delta\nu}{\Delta\nu_\odot}\right)^{-4} \left(\frac{T_{\rm eff}}{\rm T_{eff,\odot}}\right)^{1.5}, \quad (3)$$

making the results less sensitive to systematic uncertainties in $T_{\rm eff}$.

For both Eqs. 2 and 3, it is known that one needs to apply a correction to $\Delta\nu$ in order to obtain a correct mass (Sharma et al. 2016). This comes from the fact that Eq. 2 is an approximate relation, but stellar models can quantify the approximation for a given star. Here we use the correction software *asfgrid*[5] by Sharma et al. (2016) to make the appropriate corrections. For the targets selected using our selection criteria (Sec. 2), the correction is usually within 2%.

Because the SONG observations of our four new stars are short and single-site, $\Delta\nu$ cannot be determined. However, we have long enough time-series for γ Cep (both single-site and dual-site) from SONG and for 24 Sex from TESS to measure their $\Delta\nu$.

5.1 γ Cep

Despite the difficulty of measuring $\Delta\nu$ in red giants from ground-based data, our single-site and dual-site data of γ Cep provide an opportunity to do so. For this purpose, we combined those two data sets by multiplying their respective power density spectra, thus retaining the peaks similar in both spectra while reducing the power of those that are not in common. The resulting power density spectra are shown in Fig. 6.

We performed an autocorrelation on the combined power density spectrum to search for regularity. The peak at the frequency shift for which the correlation is the strongest in the vicinity of the $\Delta\nu$ predicted from the $\Delta\nu$ - $\nu_{\rm max}$ relation (Stello et al. 2009), is taken as the $\Delta\nu$ peak, and its FWHM gives a conservative uncertainty in $\Delta\nu$. We obtained a $\Delta\nu$ of 14.28 ± 0.58 μHz, as can be seen from Fig. 7.

Although the autocorrelation allows us to detect $\Delta\nu$, it does so only marginally and does not give any information about where the underlying modes are located in the spectrum. To investigate the regularity in the power density spectrum further, we divided it into segments of length equal to a trial $\Delta\nu$ and stacked them on top of one another. When the trial $\Delta\nu$ corresponded to the correct large frequency separation of the stellar oscillations, modes of the same degree aligned vertically with each other. This diagram, known as an échelle diagram (Grec et al. 1983; Bedding & Kjeldsen 2010), allowed us to clearly see which $\Delta\nu$ provided alignment (a repeated pattern) and showed the absolute location of the aligned peaks. We use the *echelle*[6] module (Hey 2019) to plot the échelle diagrams and test the trial $\Delta\nu$ for which the peaks align vertically. From *Kepler* data, we know there is a correlation between $\Delta\nu$ and the location of the aligned peaks in the échelle diagram (White et al. 2011), which is tighter for red giants (see also Bedding & Kjeldsen 2010, Huber et al. 2010, and Mosser et al. 2010) compared to less evolved stars. Hence, the $\Delta\nu$ that we find needs to agree with the correct location of the aligned peaks.

For γ Cep, we tested values of $\Delta\nu$ from 0 to 20 μHz. We found that the peaks stacked neatly on top of one another when $\Delta\nu$ = 14.25 μHz (Fig. 8a), which is consistent with our results from the

[5] https://ascl.net/1603.009

[6] https://pypi.org/project/echelle/

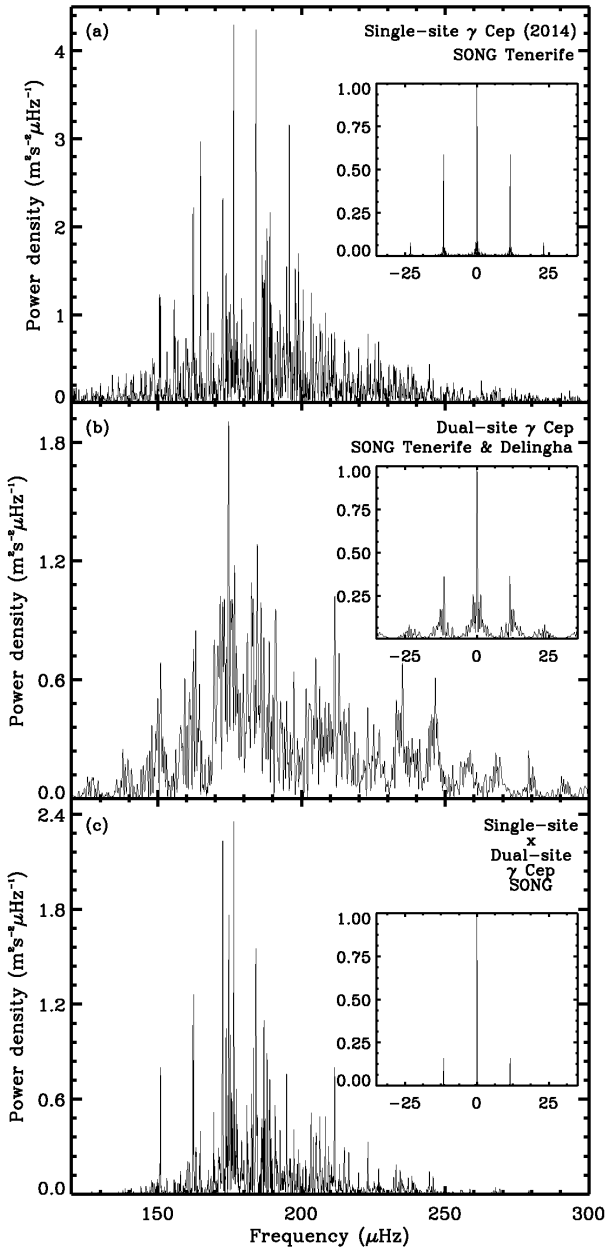

Figure 6. (a) Power density spectrum of single-site γ Cep observations (b) Power density spectrum of dual-site γ Cep data (c) Combined power density spectrum of both γ Cep spectra

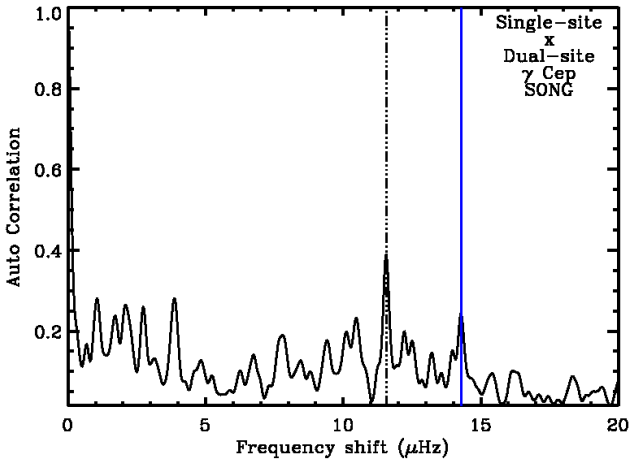

Figure 7. Autocorrelation of the combined power density spectra for γ Cep. The dash-dot line represents the daily alias of 11.574 μHz (1 cycle per day). The solid blue line represents the observed $\Delta\nu$.

Table 4. Approximate frequencies of individual modes extracted from the échelle diagrams of γ Cep and 24 Sex

γ Cep		24 Sex	
Estimated Frequency (μHz) (1)	Expected Mode (2)	Estimated Frequency (μHz) (3)	Expected Mode (4)
162.5	$l = 0$	158.8	$l = 0$
176.5	$l = 0$	172.5	$l = 0$
190.8	$l = 0$	186.8	$l = 0$
205.1	$l = 0$	201.0	$l = 0$
174.7	$l = 2$	184.3	$l = 2$
189.0	$l = 2$	199.2	$l = 2$
203.4	$l = 2$	213.1	$l = 2$
172.6	$l = 1$ (alias)	194.1	$l = 1$
184.1	$l = 1$		

autocorrelation. For comparison, we plot the échelle diagram of the *Kepler* star *KIC* 6838375, which has a similar $\Delta\nu$ and $\nu_{\rm max}$ as γ Cep (Yu et al. 2018) (Fig. 8b). The long continuous time-base of the *Kepler* data enables us to see the oscillations and identify the modes clearly. We find that the $\Delta\nu$ observed for γ Cep creates an échelle similar to that of the representative star observed by *Kepler* (e.g. aligned peaks at similar locations), except at much lower resolution (due to the shorter time series) and with alias peaks present (due to the non-continuous data of SONG). The latter makes it difficult to determine with certainty whether the peaks in the dipole region are real or aliases. We find one peak that is probably real based on its strength and the location in the échelle as well as the location of the peak that we identify as its alias (white triangle). The approximate frequencies for the individual mode frequencies extracted from the échelle diagram are listed in Table 4.

For γ Cep, we obtain a mass of 1.37 ± 0.15 $M_\odot$ when using $\Delta\nu$ alone (from Eq. 2) and a mass of 1.20 ± 0.22 $M_\odot$ when both $\Delta\nu$ and $\nu_{\rm max}$ are used (Eq. 3). These were both in agreement with its previously published $\nu_{\rm max}$-based mass (Stello et al. 2017) even when adopting our new, much smaller $\nu_{\rm max}$ uncertainties for the Stello et al. (2017) results (Table 3).

5.2 24 Sex

Compared to ground-based observations, it is relatively easy to measure $\Delta\nu$ in space-based observations due to the availability of continuous data and hence, lower aliases. The 25-day long TESS data for one of the stars in our sample, 24 Sex, therefore enables us to measure its $\Delta\nu$.

As for the SONG data of γ Cep, we first calculated the auto-correlation of the power density spectrum of the TESS data for 24

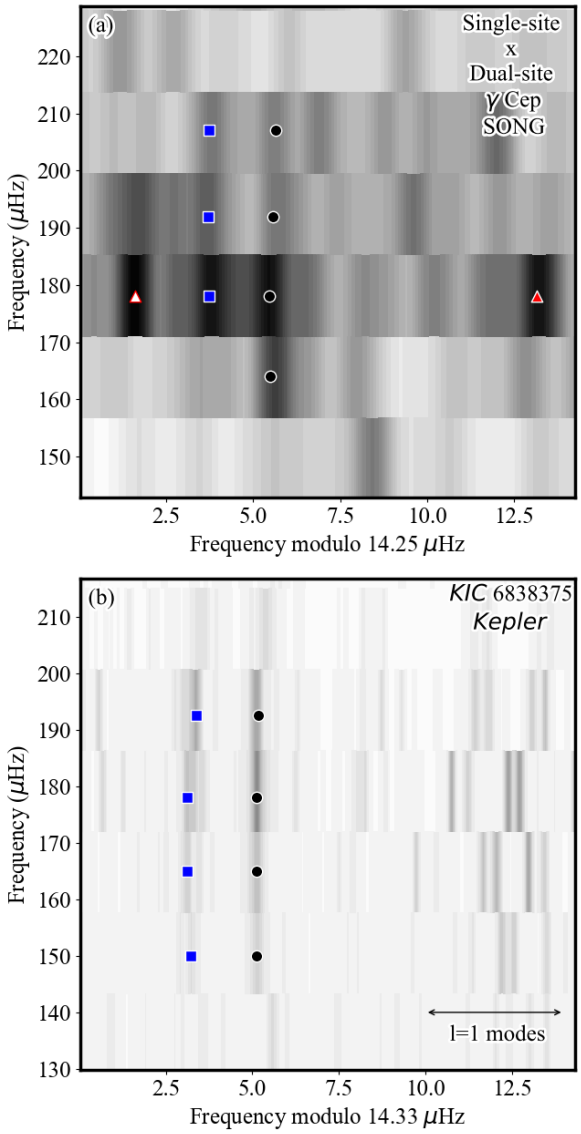

Figure 8. (a) Échelle diagram of γ Cep computed from the combined smoothed power density spectrum. The filled black circles mark the radial ($l = 0$) mode frequencies. The filled blue squares represent the quadrupole ($l = 2$) modes. The filled red triangle represents a dipole ($l = 1$) mode while the white-filled red triangle represents its alias. Only the modes, which could be clearly distinguished based on their strength and location, are marked. The approximate frequencies corresponding to these modes are provided for reference in Table 4 (columns 1 and 2). (b) Échelle diagram of the *Kepler* star *KIC* 6838375, which has a $\Delta\nu$ similar to γ Cep. Here we mark the region where the strongest dipole modes fall.

Sex. Fig. 9 indicates a strong correlation for a frequency spacing of 14.15 ± 1.23 μHz. We find the best vertical alignment of the modes in the échelle diagram for a $\Delta\nu$ = 14.10 μHz (Fig. 10).

We obtain a mass of 1.39 ± 0.23 $M_\odot$ for 24 Sex based on $\Delta\nu$ (Eq. 2), and 1.64 ± 0.38 $M_\odot$ using both $\Delta\nu$ and ν_{max}. These results are consistent with the ν_{max}-based mass from SONG that we report in Table 2 and hence also lower than the spectroscopic mass.

Overall, we see that the ν_{max}-, $\Delta\nu$- and the '$\Delta\nu$ + ν_{max}'-based masses are in good agreement with each other.

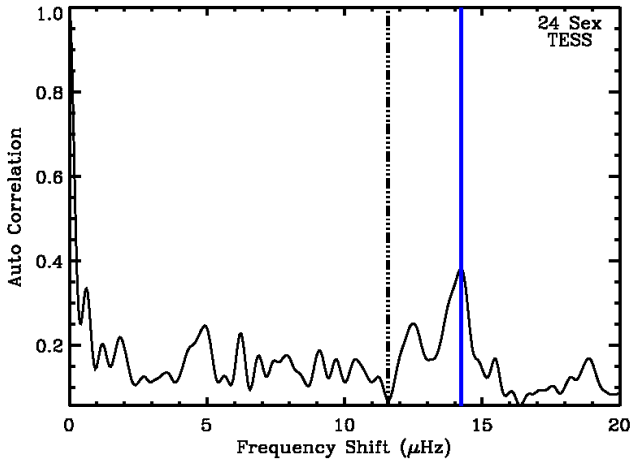

Figure 9. Autocorrelation of the power density spectrum for 24 Sex from TESS data. The dash-dot line represents the daily alias of 11.574 μHz (1 cycle/day), the solid blue line represents the observed $\Delta\nu$.

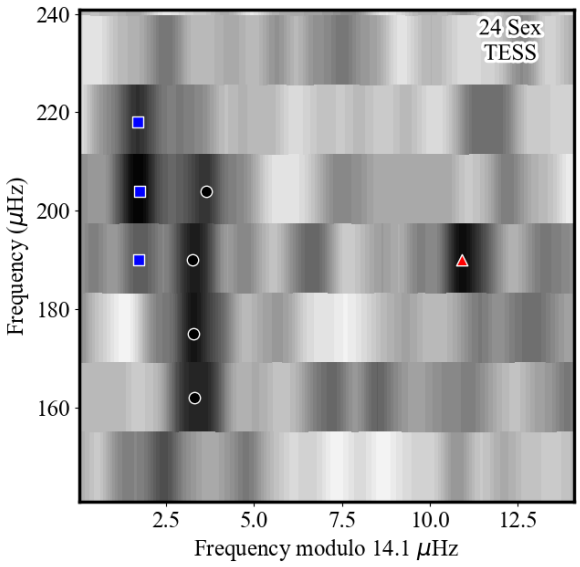

Figure 10. Échelle diagram from the TESS data for 24 Sex. The filled black circles mark the radial mode frequencies ($l = 0$), the filled blue squares represent the quadrupole ($l = 2$) modes and the filled red triangle represents a dipole ($l = 1$) mode. Like for γ Cep, only the modes, which could be clearly distinguished based on their strength and location, are marked. The approximate frequencies corresponding to these modes are provided in Table 4 (columns 3 and 4).

6 OFFSET BETWEEN THE SPECTROSCOPIC AND SEISMIC MASSES

From Table 2, we see all four new stars presented here show seismic masses lower than the spectroscopic masses from the Exoplanet Orbit Database. This agrees with the results on seven stars from Stello et al. (2017) but disagrees with the results from North et al.

(2017) and the one star in the Stello et al. (2017) sample (γ Cep), for which the seismic and spectroscopic masses agree.

To further investigate these apparent inconclusive results, we combine all the results from the previous papers (Stello et al. 2017; North et al. 2017) with ours, only choosing the stars for which the sources for spectroscopic mass are the same, for consistency. We show in Fig. 11a the mass difference ($M_{\rm seis}$-$M_{\rm spec}$) as a function of the spectroscopic mass ($M_{\rm spec}$) for the largest sample of stars (16 stars) with a single spectroscopic source (Mortier et al. 2013). This combined data shows an interesting trend. The difference between the two mass scales is insignificant for low mass stars, in agreement with the results by North et al. (2017) (and the lowest mass star by Stello et al. 2017). However, for the more massive stars, the difference between the two scales is pronounced, which agrees with the conclusions made by Stello et al. (2017). Here we note that the majority of stars investigated by North et al. (2017) are of lower mass than those investigated by Stello et al. (2017). We observe a sudden increase in the offset between the two mass scales at about 1.6 $M_\odot$. This increasing offset with mass persists even when we adopt spectroscopic masses from Jofré et al. (2015) and Brewer et al. (2016), which are the second- and the third-largest sample (15 and 13 stars) respectively we could obtain from a single source (Fig. 11b and c). Of the planet-hosting subgiants studied by Johnson et al. (2010), the massive stars ($M \gtrsim 1.6$ $M_\odot$) constitute $\sim 46\%$, which contribute to their planet occurrence-mass-metallicity correlation. Correcting for the observed mass-dependent offset would push the retired A-star sample to smaller masses, which would result in a steeper planet occurrence as a function of stellar mass compared to what was presented by Johnson et al. (2010, Eq. 8). A recalculation of the planet occurrence is beyond the scope of the current paper but will be derived in future work (Malla et al. in prep.).

Given that our seismic masses $M_{\rm seis}$ plotted in Fig. 11 are based on $\nu_{\rm max}$, one could suspect that Eq. 1 provides biased results; either because the different quantities that go into the relation ($T_{\rm eff}$, L, $\nu_{\rm max}$) are biased or because the relation itself breaks down. However, Stello et al. (2017) previously studied the effect of the potential systematics on $\nu_{\rm max}$. They determined the adopted $T_{\rm eff}$ was unlikely to be off by enough to affect the $\nu_{\rm max}$ by such a significant amount as the mass offset we see beyond 1.6 $M_\odot$ (this is also supported by our consistent masses from Eqs. 1, 2, and 3, given their different dependence on $T_{\rm eff}$). They noted that a systematic shift in metallicity by 0.1 dex only alters the $\nu_{\rm max}$ predicted from spectroscopy by 4% for stars on the red giant branch. They also found it highly unlikely for the $\nu_{\rm max}$ scaling relations to be off by 15-20% for red giants. They concluded that the potential systematics only affected the $\nu_{\rm max}$ by 4-5%, which is within our adopted uncertainty. Thus, it seems safe to assume the potential systematics in the seismic mass does not cause the observed offset. This has subsequently been supported by the comparison of radii and masses based on Eqs. 1 and 2 with results from Gaia (Zinn et al. 2019) and Galactic stellar populations (Sharma et al. 2019), suggesting even less room for error in Eq. 1. The sudden jump in stellar rotation speeds, Kraft break, occurs at 1.2 $M_\odot$ (Kraft 1967), and thus, the observed offset is unlikely to be a result of this jump in rotational velocities either.

The transition mass of 1.6 $M_\odot$ for the offset is about the same as the one that separates slow- and fast-evolving stars in the lower red giant branch region, which is where most of our 'retired A-star' targets lie. From Fig. 1, it is clear that massive stars ($M \gtrsim 1.6$ $M_\odot$) evolved much faster (thus spend less time) in the target region. Given the size of the spectroscopy-based uncertainties and the merging of tracks of different masses on the red giant branch, the typical spectroscopic error box can easily encompass low mass

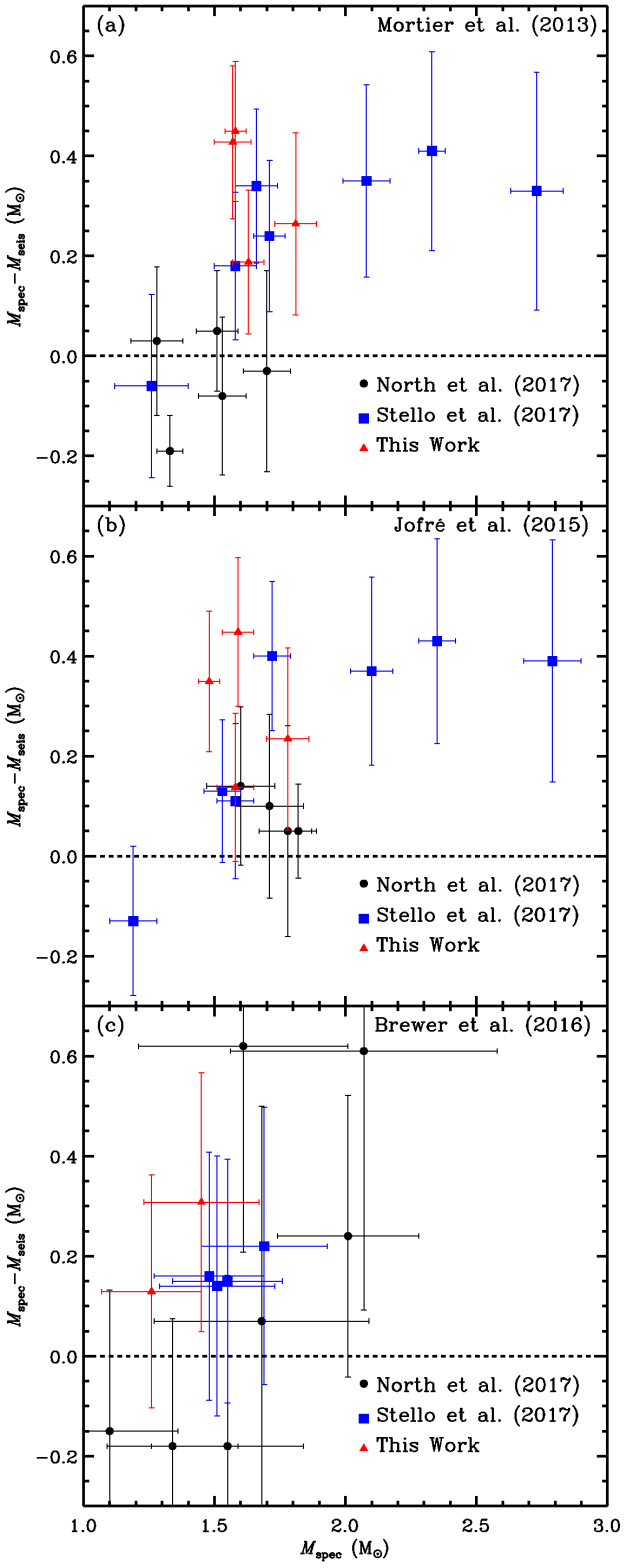

Figure 11. Difference between the spectroscopic and seismic masses plotted as a function of spectroscopic mass from source: (a) Mortier et al. (2013) (16 stars) (b) Jofré et al. (2015) (15 stars) (c) Brewer et al. (2016) (13 stars). The results from Stello et al. (2017) with updated error bars and North et al. (2017) have also been included. The filled red triangles represent the results obtained from this paper, the filled black circles represent the results from North et al. (2017), and the filled blue squares denote the results from Stello et al. (2017). We note that the overlap between our full seismic sample and the spectroscopic sample of Brewer et al. (2016) only has stars less than 2.1 $M_\odot$.

(slow and hence more likely) and high mass (fast and hence less likely) evolving tracks at the same time. Therefore, if the evolution speeds are not properly accounted for, the inferred stellar masses can be easily overestimated (Lloyd 2011).

7 CONCLUSIONS

We used radial velocity time-series from the ground-based SONG telescopes to determine the asteroseismic masses of four evolved planet-hosting stars that have previously not been investigated using asteroseismology. Our observations are too short to enable the measurement of the large frequency separation or individual mode frequencies. With especially long or less interrupted data for γ Cep (a star previously reported by Stello et al. 2017) and 24 Sex (a star from our sample), we were able to establish the robustness of the results that were based on the shorter base-line data by independently estimating the stellar mass from $\Delta\nu$ alone and from $\Delta\nu$ and $\nu_{\rm max}$ combined.

We found an offset between the spectroscopic and seismic mass scales above a transition mass of 1.6 $M_\odot$. Our results are consistent with North et al. (2017) who found no offset for less massive stars and with Stello et al. (2017) who found an offset for more massive stars. Our results also agree with the more recent result by Campante et al. (2019) who found a TESS-based seismic mass of 1.23 ± 0.15 $M_\odot$ against a spectroscopic mass of 2.1 ± 0.1 $M_\odot$ for the evolved planet-host HD 203949. These results suggest that the spectroscopy-based stellar masses of massive stars ($M \gtrsim 1.6$ $M_\odot$) are prone to overestimation, which implies that planet occurrence increases even more steeply with host star mass, compared to previous estimates (Johnson et al. 2010; Ghezzi et al. 2018).

TESS is currently observing many of these evolved planet-hosting stars, which will enable us to measure their $\nu_{\rm max}$, and possibly $\Delta\nu$ and individual mode frequencies. By combining these data with the Gaia DR2 parallax measurements, we should be able to get more precise mass estimates for an even larger sample of previously reported evolved planet hosts that bracket the mass around the transition mass to further confirm our finding.

ACKNOWLEDGEMENTS

We would like to acknowledge the Villum Foundation, The Danish Council for Independent Research | Natural Science and the Carlsberg Foundation for the support on building the SONG prototype on Tenerife. This research is based on observations made with the SONG telescopes operated on the Spanish Observatorio del Teide (Tenerife) and at the Chinese Delingha Observatory (Qinghai) by the Aarhus and Copenhagen Universities, by the Instituto de Astrofísica de Canarias and by the National Astronomical Observatories of China. Funding for the Stellar Astrophysics Centre is provided by The Danish National Research Foundation (Grant agreement no.: DNRF106). D.S. acknowledges support from Australian Research Council. D.H. acknowledges support by the National Science Foundation (AST-1717000). This research had made use of the Exoplanet Database and the Exoplanet Data Explorer at exoplanets.org. This research also uses data collected by the TESS mission, which is funded by NASA Explorer program and obtained from the Mikulski Archive for Space Telescopes (MAST). STScI is operated by the Association of Universities for Research in Astronomy, Inc., under NASA contract NAS5-26555. Support for MAST for non-HST data is provided by the NASA Office of Space Science via grant NNX13AC07G and by other grants and contracts. In addition, this research has made use of NASA's Astrophysics Data System Bibliographic Services.

REFERENCES

Alonso A., Arribas S., MartÃŋnez-Roger C., 1999, Astronomy and Astrophysics Supplement Series, 140, 261
Andersen M. F., et al., 2014. pp 83–86, http://adsabs.harvard.edu/abs/2014RMxAC..45...83A
Andersen M. F., Grundahl F., Beck A. H., Pallé P., 2016, in Revista Mexicana de Astronomia y Astrofisica Conference Series. pp 54–58 (arXiv:1901.08293)
Antoci V., et al., 2013, Monthly Notices of the Royal Astronomical Society, 435, 1563
Arentoft T., et al., 2019, Astronomy & Astrophysics, 622, A190
Basu S., Chaplin W. J., 2018, Asteroseismic data analysis: foundations and techniques. http://dx.doi.org/10.23943/princeton/9780691162928.001.0001
Bedding T. R., Kjeldsen H., 2010, Communications in Asteroseismology, 161, 3
Bovy J., Rix H.-W., Green G. M., Schlafly E. F., Finkbeiner D. P., 2016, The Astrophysical Journal, 818, 130
Brewer J. M., Fischer D. A., Valenti J. A., Piskunov N., 2016, ApJS, 225, 32
Brown T. M., Gilliland R. L., Noyes R. W., Ramsey L. W., 1991, The Astrophysical Journal, 368, 599
Butler R. P., Marcy G. W., Williams E., McCarthy C., Dosanjh P., Vogt S. S., 1996, Publications of the Astronomical Society of the Pacific, 108, 500
Campante T. L., et al., 2017, Monthly Notices of the Royal Astronomical Society, 469, 1360
Campante T. L., et al., 2019, arXiv e-prints, p. arXiv:1909.05961
Chaplin W. J., Miglio A., 2013, Annual Review of Astronomy and Astrophysics, 51, 353
Deng L., et al., 2012, Proceedings of the International Astronomical Union, 8, 318
Drimmel R., Cabrera-Lavers A., LÃşpez-Corredoira M., 2003, Astronomy & Astrophysics, 409, 205
Drimmel R., Bucciarelli B., Inno L., 2019, Research Notes of the American Astronomical Society, 3, 79
Frandsen S., et al., 2002, Astronomy & Astrophysics, 394, L5
Fredslund Andersen M., Handberg R., Weiss E., Frand sen S., Simón-Díaz S., Grundahl F., Pallé P., 2019, PASP, 131, 045003
Gaulme P., et al., 2016, The Astrophysical Journal, 832, 121
Ghezzi L., Montet B. T., Johnson J. A., 2018, The Astrophysical Journal, 860, 109
Grec G., Fossat E., Pomerantz M. A., 1983, Sol. Phys., 82, 55
Green G. M., et al., 2015, The Astrophysical Journal, 810, 25
Grundahl F., et al., 2017, The Astrophysical Journal, 836, 142
Hey D. R., 2019, danhey/echelle: Initial release, doi:10.5281/zenodo.3403407, https://doi.org/10.5281/zenodo.3403407
Hjørringgaard J. G., SilvaÂăAguirre V., White T. R., Huber D., Pope B. J. S., Casagrande L., Justesen A. B., Christensen-Dalsgaard J., 2017, Monthly Notices of the Royal Astronomical Society, 464, 3713
Huber D., Stello D., Bedding T. R., Chaplin W. J., Arentoft T., Quirion P.-O., Kjeldsen H., 2009, Communications in Asteroseismology, 160, 74
Huber D., et al., 2010, ApJ, 723, 1607
Huber D., et al., 2011, ApJ, 731, 94
Huber D., et al., 2012, The Astrophysical Journal, 760, 32
Huber D., et al., 2017, The Astrophysical Journal, 844, 102
Jofré E., Petrucci R., Saffe C., Saker L., Artur de la Villarmois E., Chavero C., G\'omez M., Mauas P. J. D., 2015, Astronomy & Astrophysics, 574, A50
Johnson J. A., Marcy G. W., Fischer D. A., Henry G. W., Wright J. T., Isaacson H., McCarthy C., 2006, The Astrophysical Journal, 652, 1724

Johnson J. A., Aller K. M., Howard A. W., Crepp J. R., 2010, Publications of the Astronomical Society of the Pacific, 122, 905
Johnson J. A., Morton T. D., Wright J. T., 2013, The Astrophysical Journal, 763, 53
Johnson J. A., et al., 2014, The Astrophysical Journal, 794, 15
Kallinger T., et al., 2010, Astronomy and Astrophysics, 509, A77
Kjeldsen H., Bedding T. R., 1995, Astronomy and Astrophysics, 293, 87
Kraft R. P., 1967, ApJ, 150, 551
Leeuwen F. v., 2007, Hipparcos, the New Reduction of the Raw Data. Astrophysics and Space Science Library, Springer Netherlands, //www.springer.com/gp/book/9781402063411
Lloyd J. P., 2011, The Astrophysical Journal Letters, 739, L49
Lloyd J. P., 2013, The Astrophysical Journal Letters, 774, L2
Marshall D. J., Robin A. C., ReylÃĺ C., Schultheis M., Picaud S., 2006, Astronomy & Astrophysics, 453, 635
Mortier A., Santos N. C., Sousa S. G., Adibekyan V. Z., Delgado Mena E., Tsantaki M., Israelian G., Mayor M., 2013, Astronomy and Astrophysics, 557, A70
Mosser B., et al., 2010, A&A, 517, A22
Murphy S. J., 2012, Monthly Notices of the Royal Astronomical Society, 422, 665
North T. S. H., et al., 2017, Monthly Notices of the Royal Astronomical Society, 472, 1866
Paxton B., et al., 2013, The Astrophysical Journal Supplement Series, 208, 4
Piskunov N. E., Valenti J. A., 2002, Astronomy & Astrophysics, 385, 1095
Pont F., Eyer L., 2004, Monthly Notices of the Royal Astronomical Society, 351, 487
Prieto C. A., Lambert D. L., 1999, Astronomy & Astrophysics, p. 8
Ricker G. R., et al., 2016, in Space Telescopes and Instrumentation 2016: Optical, Infrared, and Millimeter Wave. p. 99042B, doi:10.1117/12.2232071
Ritter A., Hyde E. A., Parker Q. A., 2014, Publications of the Astronomical Society of the Pacific, 126, 170
Schlaufman K. C., Winn J. N., 2013, The Astrophysical Journal, 772, 143
Sharma S., Stello D., Bland-Hawthorn J., Huber D., Bedding T. R., 2016, ApJ, 822, 15
Sharma S., et al., 2019, MNRAS, p. 2471
Stello D., Bruntt H., Preston H., Buzasi D., 2008, The Astrophysical Journal, 674, L53
Stello D., Chaplin W. J., Basu S., Elsworth Y., Bedding T. R., 2009, Monthly Notices of the Royal Astronomical Society: Letters, 400, L80
Stello D., et al., 2013, The Astrophysical Journal, 765, L41
Stello D., et al., 2017, Monthly Notices of the Royal Astronomical Society, 472, 4110
Thygesen A. O., et al., 2012, A&A, 543, A160
White T. R., Bedding T. R., Stello D., Christensen-Dalsgaard J., Huber D., Kjeldsen H., 2011, ApJ, 743, 161
White T. R., et al., 2018, MNRAS, 477, 4403
Wright J. T., et al., 2011, Publications of the Astronomical Society of the Pacific, 123, 412
Yu J., Huber D., Bedding T. R., Stello D., Hon M., Murphy S. J., Khanna S., 2018, The Astrophysical Journal Supplement Series, 236, 42
Zinn J. C., Pinsonneault M. H., Huber D., Stello D., 2019, ApJ, 878, 136

This paper has been typeset from a TEX/LATEX file prepared by the author.